Journal of Nuclear Materials 386–388 (2009) 173–176

Contents lists available at ScienceDirect

Journal of Nuclear Materials

journal homepage: www.elsevier.com/locate/jnucmat

Evaluation of radiation damages on the first-wall surface in LHD exposed to charge-exchanged helium particles

M. Tokitani [a,*], N. Yoshida [b], M. Miyamoto [c], Y. Ohtawa [b], K. Tokunaga [b], T. Fujiwara [b], S. Masuzaki [a], N. Ashikawa [a], M. Shoji [a], M. Kobayashi [a], A. Sagara [a], N. Noda [a], H. Yamada [a], A. Komori [a], LHD Experimental Group [a], S. Nagata [d], B. Tsuchiya [d]

[a] National Institute for Fusion Science, 322-6 Oroshi, Toki, Gifu 509-5292, Japan
[b] Research Institute for Applied Mechanics, Kyushu University, Kasuga, Fukuoka 816-8580, Japan
[c] Department of Material Science, Shimane University, Matsue, Shimane 690-8504, Japan
[d] Institute for Materials Research, Tohoku University, Sendai, Miyagi 980-8577, Japan

ARTICLE INFO

PACS:
52.40.Hf
25.60.Lg
52.55.−s
87.64.Ee
79.20.Rf

ABSTRACT

In order to clarify the radiation damages caused by charge-exchanged helium particles, metal specimens were inserted into the first wall position by using material probe system in LHD, and then, exposed to the neutral beam heated helium plasmas (87 s in total). After the exposure, dense helium bubbles with size of 1–2 nm and dislocation loops were confirmed in all specimens from transmission electron microscope observation. It means that the energy of incidence helium particles is sufficiently higher than that of the minimum energy for creating the knock-on damage (E_{min}). Majority of such incidence helium particles are energetic neutrals created by charge-exchange collisions [R.J. Goldston, P.H. Rutherford, Introduction to Plasma Physics, 1996, p. 156]. It was tried to estimate the flux and energy of CX-helium to the first walls by comparing with systematic helium ion irradiation experiments [H. Iwakiri et al., J. Nucl. Mater. 283–287 (2000) 1134], [M. Tokitani et al., J. Nucl. Mater. 329–333 (2004) 761]. The estimated flux and energy from size and density of the defects is the order of $\sim 10^{19}$ He/m^2 s, and about 1–2 keV, respectively.

1. Introduction

In the case of burning plasma, the first wall materials suffer heavy bombardment of helium particles generated by D-T fusion reaction. Majority of incidence helium particles are energetic neutrals (CX-neutrals) created by charge-exchange collisions [1]. It is well known that helium atoms in metals are deeply trapped by lattice defects such as vacancies and helium-vacancy complexes formed by their own irradiation. Strong irradiation effects of helium have been observed in many kinds of metals such as W and Mo including stainless steel [4–8].

The large helical device (LHD) is the largest heliotron-type plasma machine with super conducting helical magnetic coil systems [9]. Its first wall panels and divertor plates are consisted of stainless steel and isotropic graphite, respectively. The former is the major material in LHD and the graphite area is only about 5% of the total plasma facing area. It was reported that for helium plasma discharge experiments in the LHD, about half of the inlet helium was trapped in the wall, even after a long helium glow discharge cleaning [10]. Understanding of the effects of CX-helium atoms to the metal first wall is important for not only the elucidation of materials degradation but also the plasma operations in LHD. However, focused research on the material damages caused by CX-helium atoms and the evaluation of incidence energy and flux of CX-neutrals has been scarcely done so far in not only LHD but also other plasma confinement devices.

In the present study, microscopic damage and depth profile of helium in metals bombarded by CX-helium atoms during LHD helium discharges was studied by means of transmission electron microscopy (TEM) and elastic recoil detection (ERD) analysis, and then, incidence flux and energy of CX-neutrals were evaluated.

2. Experimental procedures

Pre-thinned vacuum annealed specimens of stainless steels (SUS), Mo, W and Cu were mounted on the probe head were inserted into the first wall equivalent position by using the retractable material-probe system which equipped with LHD as shown in Fig. 1. W and Mo were made by powder metallurgy and cold work. The thickness of the bulk specimen (for ERD) is 0.1 mm. Annealing temperatures of SUS, Mo, W and Cu were 1320 K,

* Corresponding author. Tel.: +81 572 58 2143; fax: +81 572 58 2618.
E-mail address: tokitani.masayuki@LHD.nifs.ac.jp (M. Tokitani).

0022-3115/$ - see front matter © 2008 Elsevier B.V. All rights reserved.
doi:10.1016/j.jnucmat.2008.12.086

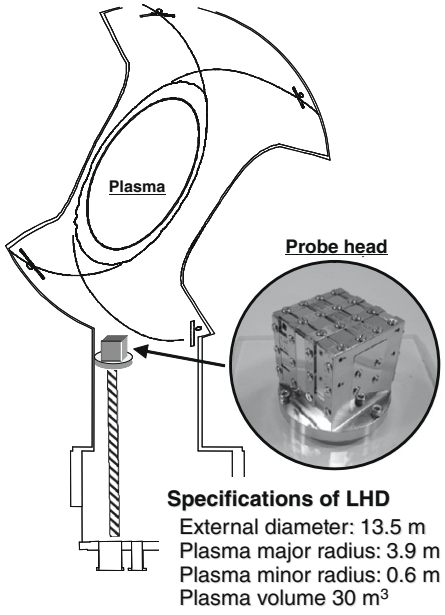

Fig. 1. Schematic view of the experimental set up in LHD.

~2273 K, ~2273 K and 873 K, respectively. They were exposed to successive helium discharges sustained by neutral beam injection (NBI). Typical plasma parameters were as follows: $T_i = 0.7$–1.7 keV, $n_e = 0.3$–8.1×10^{19} m^{-3}. The typical duration time of a discharge was about 2 s and the total reached 87 s by repeating discharges with similar plasma parameters. The temperature of the probe head during exposure was monitored by the thermocouples placed just beneath the specimens. It stayed almost constant near room temperature. Therefore, specimen temperature was kept at room temperature. After the exposure, microscopic damage of the specimens was observed by means of TEM and then, incidence flux and energy of CX-helium particles were estimated by comparing with the in situ TEM observation results under helium ion irradiation case [3].

Depth profile of the retained helium atoms were detected successfully by using the oxygen ($^{16}O^{4+}$) analyzing beam ERD technique with the energy of 5.0 MeV. Incident angle of the analyzing beam was 72° to the surface normal of the specimen. The recoiled helium atoms were detected by ERD (solid state) detector. The back scattered ^{16}O atoms were detected by Rutherford backscattering spectrometry techniques. RBS detector was placed at an angle of 170° to the incident direction. An Al film of 4 μm thick was placed in front of the ERD detector to absorb the O ions scattered from the specimen surface. Principle of this detection technique is the same as Ref. [11]. In this method, the retained helium atoms can be analyzed very clearly, because back ground signal of the measurement does not show any sign.

3. Results and discussion

3.1. Evaluation of microscopic damage

Fig. 2 shows TEM images of SUS, Mo, W and Cu specimens exposed to the NBI heated helium discharges (87 s in total). The upper series of micrographs are bright field images with large deviation parameter *s*. White dot images are helium bubbles. The lower series are dark field images with small deviation parameter *s*, which fits for observation of defects with strong lattice distortion. Defects with a strong white image, mainly dislocation loops. Although total irradiation time was only 87 s, very dense fine helium bubbles of about 1–2 nm in diameter and considerably large amounts of dislocation loops were formed in all specimens. It means that the damage is caused by CX-helium atoms which are not affected by magnetic field, and their energy and flux are sufficiently higher to create these defects. In general, radiation induced secondary defects are formed as aggregates of point defects produced by knock-on processes. For example, minimum incidence energy (E_{min}) for creating the knock-on damage to W is ~0.78 keV [12]. Due to the high damage rate, production rate of radiation damages scarcely depends on the metal components.

3.2. Estimation of the flux and energy of CX-helium atoms from microstructural evolution

Evolution of microstructure in SUS at room temperature under 2 keV helium ion irradiation is shown in Fig. 3. Some of the images are re-produced data from Ref. [3]. Small black dot defects and helium bubbles appeared at early stage, and finally they were reached to the saturation level (~10^{22} He/m^2). From comparison

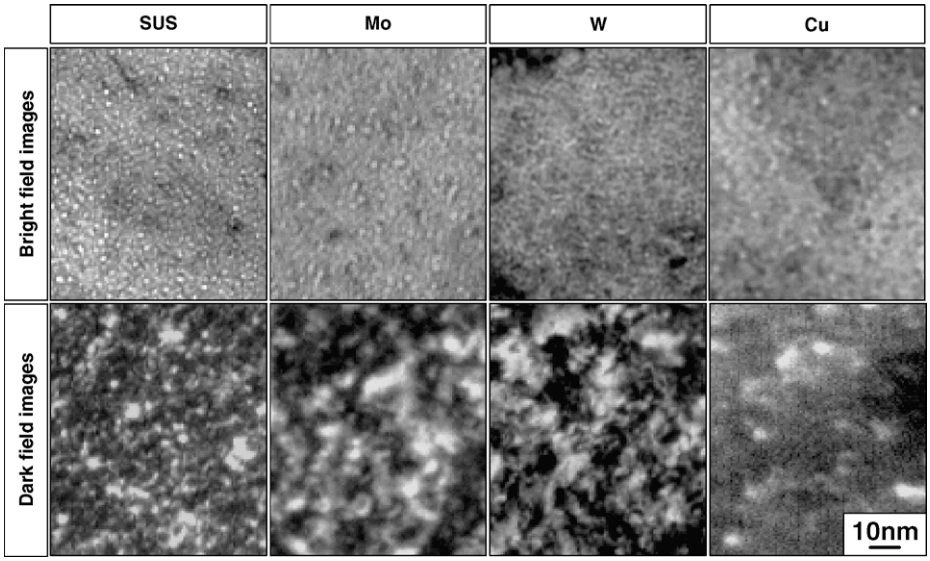

Fig. 2. Microscopic damages in SUS, Mo, W and Cu specimens exposed to the NBI heated helium discharges (87 s in total).

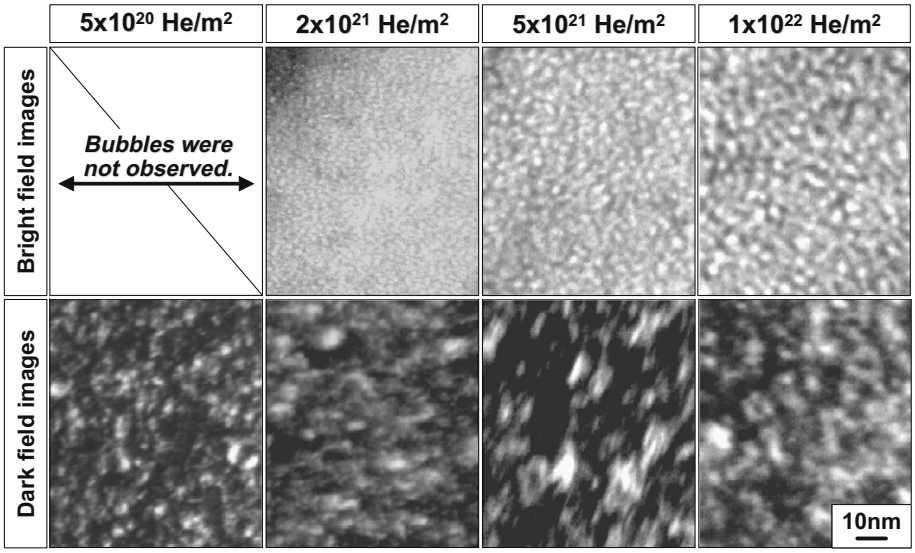

Fig. 3. Microstructural evolution in stainless steel during helium ion irradiation ($\sim 1 \times 10^{22}$ He/m^2) at room temperature with energies of 2 keV [3].

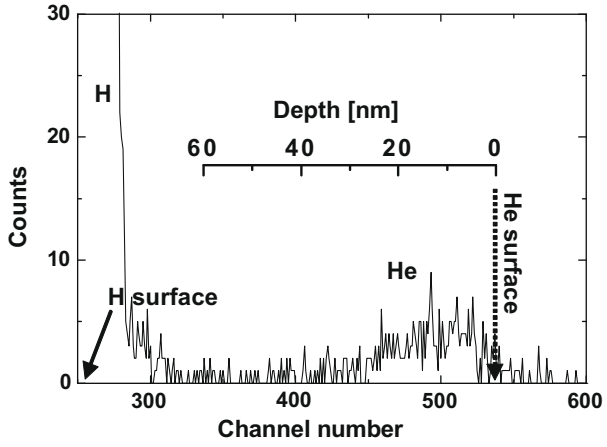

Fig. 4. ERD depth profile of retained helium atoms in W after exposed to helium discharges at first wall position.

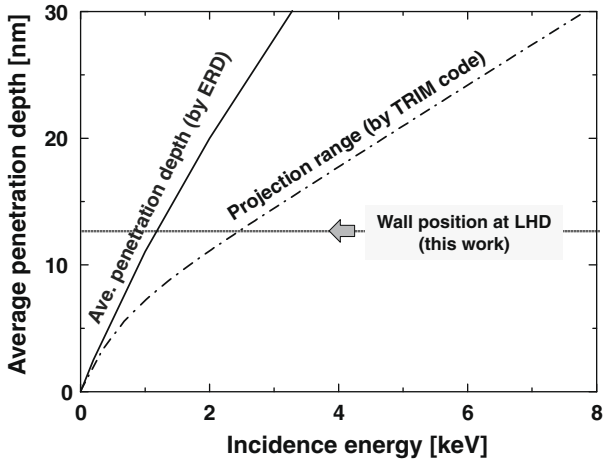

Fig. 5. Average penetration depth of injected helium atoms in W as a function of incidence energy. Dashed line is possible projection range at normal incidence angle calculated by TRIM-code. Solid line is interpolation curve of average penetration depth of helium measured by ERD after injected by ion irradiation experiments with normal incidence angle.

of Fig. 3 and LHD case (Fig. 2), it was tried to estimate the flux and energy of CX-helium atoms to the first walls. Size and density of helium bubbles and dislocation loops in LHD case corresponds to $\sim 10^{21}$ He/m^2. Therefore, the estimated flux and incidence energy is $\sim 10^{19}$ He/m^2 s and about 1–2 keV, respectively. As mentioned above, majority of such incidence helium particles are energetic neutrals. This estimation is relatively rough. However, it is important for elucidation of the CX-particle load to first walls.

It was reported that up to the dose level of $\sim 10^{20}$ He/m^2 s, injected helium atoms are trapped by vacancy-helium complex and helium bubbles and finally filled with them. Above this dose level, additional trapping of helium atoms by helium bubbles become difficult. Thus, newly injected helium is weakly trapped in the distorted lattice around high pressure bubbles and other type defects. Such weakly trapped helium was gradually detrapped at low temperature region ($\sim$500 K) [3]. Therefore, if the temperature rise occurred during discharges in the LHD first wall, helium desorption may lead to the undesired effects on plasma operations.

3.3. Depth profile of helium atoms in W

ERD depth profile of retained helium atoms in W specimen after exposed to helium discharges is shown in Fig. 4. Due to the exposure to the air during specimen transfer from LHD to the experimental facilities, hydrogen atoms seem to be absorbed on the specimen surface, and which were detected simultaneously with recoiled helium atoms. Fortunately, spectrum of recoiled helium and hydrogen atoms were successfully divided by optimization of the ERD setting as mentioned in Section 2. Since channel number of ERD spectrum corresponds to the depth, reference depth axis of helium distribution was also indicated together in this figure. It is clear that peak of the helium distribution (average penetration depth) locates at about 13 nm.

Fig. 4 shows data of average penetration depth of helium injected into W as a function of incidence energy. Dashed line is the possible projection range of injected helium atoms at normal incidence angle calculated by TRIM-code. While, solid line is the interpolation curve of average penetration depth of helium (from past experimental data) which detected by oxygen analyzing beam ERD technique after injected by ion irradiation experiments with normal incidence angle. One should note that depth profile of ERD data is distributed much deeper than that of the calculation

results of TRIM-code. The possible mechanism of such discrepancy between ERD and TRIM-code data may be related to the diffusion effect and bubble formation. These effects have not been taken into account in TRIM-code calculation. According to the ERD results (solid line), when the penetration depth of helium is 13 nm in W (see Fig. 4), majority of the CX-helium bombarding the first wall has energy of ~1 keV as illustrated in Fig. 5. Microscopic damages mentioned above are supported by this value. Incidence of such high energy CX-neutrals is serious problem for deterioration of the first wall materials in LHD. For example, it was reported that damaged region due to helium ion bombardment affected not only hardening behavior of surface but also hydrogen isotope retention [13,14].

4. Summary

Microscopic damage and helium depth profile in metals bombarded by CX-helium (neutral) atoms during LHD helium discharges was studied. From TEM observation, considerably large amounts of dislocation loops and helium bubbles of about 1–2 nm were identified in all specimens. This means that the energy of the CX-neutrals is sufficiently higher than that of the minimum energy for creating the knock-on damage (E_{min}) in all specimens. It was tried to estimate the CX-flux and energy to the first walls by comparing with in situ helium ion irradiation results in SUS [3]. The estimated CX-flux from size and density of the defects is the order of $\sim 10^{19}$ He/m^2 s, and the expected incidence energy is about 1–2 keV. While, ERD data indicate that average penetration depth of helium atoms in W locates at about 13 nm. According to the past ERD analysis (solid line in Fig. 5), when the penetration depth of helium is 13 nm in W, majority of the CX-helium bombarding the first wall has energy of ~1 keV as illustrated in Fig. 5. Generation of such high energy CX-neutrals is serious problem for deterioration of the first wall materials.

Acknowledgements

This work was performed with the support and under the auspices of the NIFS Collaborative Research Program and under the inter-university cooperative research program of the Institute for Materials Research, Tohoku University. This research was partly supported by the Japan Society for the Promotion of Science and Grant-in-Aid of Scientific Research from Japan Ministry of Education, Culture, Sports, Science and Technology.

References

[1] R.J. Goldston, P.H. Rutherford, Introduction to Plasma Phys. (1996) 156.
[2] H. Iwakiri et al., J. Nucl. Mater. 283–287 (2000) 1134.
[3] M. Tokitani et al., J. Nucl. Mater. 329–333 (2004) 761.
[4] H. Iwakiri et al., J. Nucl. Mater. 283–287 (2000) 1134.
[5] N. Yoshida, Y. Hirooka, J. Nucl. Mater. 258–263 (1998) 173.
[6] K. Ono et al., J. Nucl. Mater. 283–287 (2000) 210.
[7] D. Nishijima et al., J. Nucl. Mater. 313–316 (2003) 97.
[8] D. Nishijima et al., J. Nucl. Mater. 337–339 (2005) 927.
[9] O. Motojima et al., Nucl. Fusion 43 (2003) 1674.
[10] H. Suzuki et al., J. Nucl. Mater. 313–316 (2003) 297.
[11] S. Nagata et al., J. Nucl. Mater. 307–311 (2002) 1516.
[12] R.N. Stuart et al., Radiat. Eff. Def. Solids 30 (3) (1976) 129.
[13] H. Iwakiri et al., J. Nucl. Mater. 258–263 (1998) 873.
[14] H. Iwakiri et al., J. Nucl. Mater. 307–311 (2002) 135.